

Quantum Anomalous Hall Effect in Magnetic Topological Insulator GdBiTe_3

Hai-Jun Zhang, Xiao Zhang & Shou-Cheng Zhang

¹*Department of Physics, McCullough Building, Stanford University, Stanford, CA 94305-4045*

The quantum anomalous Hall (QAH) state is a two-dimensional bulk insulator with a non-zero Chern number in absence of external magnetic fields. Protected gapless chiral edge states enable dissipationless current transport in electronic devices. Doping topological insulators with random magnetic impurities could realize the QAH state, but magnetic order is difficult to establish experimentally in the bulk insulating limit. Here we predict that the single quintuple layer of GdBiTe_3 film could be a stoichiometric QAH insulator based on *ab-initio* calculations, which explicitly demonstrate ferromagnetic order and chiral edge states inside the bulk gap. We further investigate the topological quantum phase transition by tuning the lattice constant and interactions. A simple low-energy effective model is presented to capture the salient physical feature of this topological material.

Recently time-reversal-invariant topological insulators (TIs) have attracted broad attention in fields of the condensed matter physics, material science and electrical engineering¹⁻⁴. Quantum spin Hall (QSH) insulators^{5,6} are two dimensions (2D) TIs with a bulk energy gap and gapless helical edge states which are protected by the Z_2 topological invariant⁷. Both 2D and 3D TIs are natural platforms to realize the QAH when the time-reversal symmetry is spontaneously broken by the ferromagnetic order⁸⁻¹¹. The QAH state is the quantum version of the intrinsic anomalous

Hall effect¹², and is characterized by a bulk 2D Chern number and gapless chiral edge states without the external magnetic field^{8,13,14}, and is sometimes also referred to as the 2D Chern insulator. The QSH state has two counter-propagating edge states; doping the 2D TIs with magnetic impurities could break the time reversal symmetry, annihilate one edge state and leave the other intact, thus realizing the QAH state with chiral edge state. Alternatively, doping the surface of 3D TIs with magnetic impurities breaks time reversal symmetry, and opens up a gap for the Dirac surface states^{11,15,16}. Chiral edge states exist on the magnetic domain walls on the surface¹¹. In the QAH state, electrons move like cars on a highway, where oppositely moving traffics are spatially separated into opposite lanes¹. Realizing such a dissipationless transport mechanism without extreme condition could greatly improve the performance of electronic devices.

Normally, ferromagnetic order among magnetic impurities in randomly doped semiconductors are mediated by the free carriers¹⁷, it is difficult to establish magnetic order in the bulk insulating limit. For this reason, we search for stoichiometric ferromagnetic insulators with a nonzero Chern number for the 2D band structure. Rare earth elements have partially filled **f** electrons, in particular, Gd³⁺ has exact half filled **f** electrons. It is possible to realize a stoichiometric QAH insulator by replacing Bi by Gd in the Bi₂Te₃ family of TIs¹⁸⁻²¹. GdBiTe₃ has a stable structure phase, synthesized thirty years ago²². In this work, we predict that stoichiometric QAH insulators could be realized in the single quintuple layer(SQL) of GdBiTe₃, based on *ab-initio* calculations.

Crystal structure and band structure

GdBiTe₃ has a rhombohedral crystal structure with the space group $R\bar{3}m$. Its crystal consists

of close-packed layers stacked along [111] direction with the A-B-C... order. The quintuple layer (QL) (Te-X-Te-X-Te) structure is the basic crystal unit, where X presents Bi and Gd with a certain pattern, similar to the case of LaBiTe_3 ²¹. It has strong coupling within one QL and weak van der Waals coupling between neighbor QLs, so this material can be grown as two-dimensional (2D) thin film along [111] direction. In addition, though its lattice type and lattice constant have been measured experimentally²², positions of Bi and Gd have not been clearly resolved yet. Since Bi and Gd have different electronegativity, it is possible to grow the non-mixing structure as Te-Gd-Te-Bi-Te with Molecular beam epitaxy (MBE) technique. This crystal structure of GdBiTe_3 is shown in Fig. 1a. It holds the three-fold rotation symmetry C_3 with z axis as the trigonal axis and the reflection symmetry with x axis as its normal axis. Compared with Bi_2Te_3 ¹⁸, the inversion symmetry is broken for this structure. Since SQL GdBiTe_3 film is the simplest system to study the QAH effect, in this work we focus on its SQL structure with Te1-Bi-Te2-Gd-Te1', where Te1 and Te1' are marked for the Te closest to Bi and Gd layer separately, and Te2 denotes the Te in the center of this SQL.

All *ab-initio* calculations are carried out in the framework of density functional theory (DFT) with Perdew-Burke-Ernzerhof-type generalized-gradient approximation²³. Both BSTATE package²⁴ with plane-wave pseudo-potential method and the *Vienna ab initio simulation package* (VASP) with the projected augmented wave method are employed. The \mathbf{k} -point grid is taken as $12 \times 12 \times 1$, and the kinetic energy cutoff is fixed to 340eV in all self-consistent calculations. A free standing slab model is employed with SQL. Its lattice constant ($a = 4.16\text{\AA}$) is taken from experiments²², and the inner atomic positions are obtained through the ionic relaxation with the force cutoff

0.001eV/Å. The spin-orbit coupling (SOC) is taken into account, because of its importance to realize the QAH effect. GGA+U method²⁵ is also employed to study the strong correlation effect in GdBiTe₃ because of the existence of narrow occupied **f** bands of Gd. We find that the ferromagnetic phase is more stable than the non-magnetic and collinear anti-ferromagnetic phases for SQL GdBiTe₃. In addition, the ferromagnetic phase with magnetic moment along [111] direction has lower energy than that with the magnetic moment along [010] and [110] directions. All GdBiTe₃ calculations are carried out here with the ferromagnetic moments along [111] direction.

The ferromagnetic phase of SGL GdBiTe₃ is an insulator state with exact magnetic moment $S = 7/2$. Because of the lattice similarity between GdBiTe₃ and GdN(or EuO) with [111] direction, the known magnetic exchange mechanisms in GdN or EuO could provide possible explanation for the ferromagnetic state in SQL GdBiTe₃. The first mechanism is a third-order perturbation process²⁶. A virtual excitation, which takes a 4**f** to a 5**d** state, leads to a **f-f** interaction through the **d-f** exchange due to the wave-function overlap between neighboring rare-earth atoms. Recently, Mitra and Lambrecht²⁷, based on *ab-initio* calculations, presented another magnetic mechanism for the ferromagnetic ground state in GdN. The anti-ferromagnetic ordering, between N **p** and Gd **d** small magnetic moments, stabilizes the ferromagnetic structure between nearest neighbor Gd atoms due to the **d-f** exchange interaction. In addition, our calculations also indicate the similar anti-ferromagnetic ordering between Te **p** and Gd **d** small magnetic moments.

Bi₂Te₃, LaBiTe₃ and GdBiTe₃ have very similar SQL structure. First of all, Bi₂Te₃ have both the inversion symmetry and the time-reversal symmetry. However, inversion symmetry is broken

in LaBiTe_3 , and both inversion symmetry and time-reversal symmetry are broken in GdBiTe_3 . The band evolution from Bi_2Te_3 to LaBiTe_3 , and finally to GdBiTe_3 is shown in Fig. 1c-e. The bands of Bi_2Te_3 have double degeneracy because of both inversion and time-reversal symmetries. Its energy gap is calculated to be about 0.19eV , consistent with the experiments²⁸. The bottom of the conduction bands at Γ point with a “V” shape originates from the $p_{x,y}$ orbitals of Bi, Te1 and Te1'. The top of the valence band at the Γ point, which lies below valence bands at other momenta, originates from the $p_{x,y}$ orbitals of Te2. For LaBiTe_3 , the double degeneracy of the bands is lifted except at the time-reversal points, due to the lack of the inversion symmetry. Though the bottom of conduction bands still shows the “V” shape, the top of the valence bands moves to Γ , which mainly originates from the $p_{x,y}$ orbitals of Te2 and Te1'. The schematic evolution of the top of valence bands and the bottom of conduction bands from LaBiTe_3 to GdBiTe_3 is shown in Fig. 2a-b. The Kramers double degeneracy at the Γ point in GdBiTe_3 is broken due to the lack of time-reversal symmetry. The band inversion occurs between the $|p_x + ip_y, \text{Bi} + \text{Te1}, \downarrow\rangle$ and $|p_x + ip_y, \text{Te1}' + \text{Te2}, \uparrow\rangle$ due to the strong SOC and the large magnetic moment. The existence of this band inversion is the key point to realize the QAH effect in this SQL GdBiTe_3 system.

Fig. 3a shows that the energy gap is quite sensitive with the lattice constant. Smaller lattice constant a increases the band inversion. Conversely, increasing the lattice constant a would destroy the band inversion. The QAH effect exists for $a < 1.008a_0$, where a_0 is the experimentally determined bulk lattice constant. Because the SQL GdBiTe_3 is very thin, its lattice constant could be controlled by the substrate, giving us a broad tunability range. In addition, due to the narrow \mathbf{f} bands, the strong correlation needs to be checked by GGA+U calculations. First of all, the band

structure calculations show that the occupied \mathbf{f} bands are located at $-6eV$ below Fermi level (FL), and the unoccupied \mathbf{f} bands are located at $2.5eV$ above FL. Since both occupied and unoccupied \mathbf{f} bands are quite far from FL, correlation effects should not influence bands very close to the Fermi level. Our calculations indicate that this conclusion is true. The dependence of the energy gap on U (from $0eV$ to $8eV$) is shown in Fig. 3b. The correlation U lifts up the top spin-down valence band, and pulls down the bottom spin-up valence band. Therefore, the strong correlation U likes to pull $GdBiTe_3$ from the topologically non-trivial QAH phase to the topologically trivial ferromagnetic insulator phase. But the energy gap is much more sensitive with the lattice constant than with the correlation U . We have shown that the SQL $GdBiTe_3$ is close to the quantum critical point between the QAH state and topologically trivial magnetic insulator state, and it is possible to realize the QAH state by tuning the lattice constant with proper substrates. Also the 2D Dirac-type band dispersion shows up at the critical point, shown in Fig. 3c. This is very similar to the case of QSH state at the critical point⁵.

Topological chiral edge states

The existence of topologically protected chiral edge states is the direct and intrinsic evidence of the QAH phase. It is important to show the explicit features of these topologically protected chiral edge states. In order to calculate the edge states, we employ the tight-binding method based on maximally localized Wannier functions (MLWF), developed by Vanderbilt and his co-workers²⁹, in the framework of *ab-initio* calculations. The edge with $Te1'$ and Bi terminated along the [11] direction is chosen to show the edge states, shown in the inset of Fig. 4b. Because the topological

nature is completely determined by its bulk electronic structure, here we ignore the edge reconstruction of the atoms on the edge, and also make another approximation that the MLWF hopping parameters close to the edge are the same to ones of the bulk. The bulk MLWF hopping parameters are obtained from the *ab-initio* calculations of the SQL free-standing GdBiTe₃ slab. Similar to the method described in our previous work¹⁸, we use an iterative method³⁰ to obtain the edge Green's function of the semi-infinite system with an edge along [11] direction. The local density of states (LDOS) can be calculated with the imaginary part of these edge Green's functions, shown in Fig. 4a,b. The LDOS in Fig. 4a shows two edge states for topologically non-trivial GdBiTe₃ with the experimental lattice constant a_0 . One topologically trivial edge state only stays within the valence bands, while the topologically non-trivial edge state ties the conduction band with the valence band. This topologically non-trivial edge state is chiral, and its Fermi velocity in the energy gap is $v_F \simeq 3.1 \times 10^5 m/s$ (or $3.86 eV \cdot Bohr$). The edge states of topologically trivial ferromagnetic GdBiTe₃ with the lattice constant $a = 1.02a_0$ are shown in Fig. 4b. Both of these two topologically trivial edge states only stay within the valence bands, and do not connect the valence and conduction bands.

Low-energy effective model

As the topological nature is determined by the physics near the Γ point for this material, it is possible to write down a four-band effective Hamiltonian to characterize the low-energy long-wavelength properties of the system. Starting from the four low-lying states $|B_-, -\frac{1}{2} \uparrow\rangle = c_1|p_x - ip_y, Te1, \uparrow\rangle + c_2|p_x - ip_y, Bi, \uparrow\rangle$, $|B_+, \frac{1}{2} \downarrow\rangle = c_1|p_x + ip_y, Te1, \downarrow\rangle + c_2|p_x + ip_y, Bi, \downarrow\rangle$,

$|T_+, \frac{3}{2} \uparrow\rangle = d_1|p_x + ip_y, Te2, \uparrow\rangle + d_2|p_x + ip_y, Te1', \uparrow\rangle$ and $|T_-, -\frac{3}{2} \downarrow\rangle = d_1|p_x - ip_y, Te2, \downarrow\rangle + d_2|p_x + ip_y, Te1', \uparrow\rangle$ at the Γ point, where c_1, c_2, d_1 and d_2 are constants and $\pm\frac{1}{2}(\frac{3}{2})$ are the angular momenta in z direction. In addition, the “ \pm ” subscripts are used to present the z component of orbital angular momentum $l_z = \pm 1$. Such a Hamiltonian can be constructed by the theory of invariants for the finite wave vector \mathbf{k} . On the basis of the symmetries of the system, the generic form of the 4×4 effective Hamiltonian can be constructed up to the order of $O(k^2)$, and the parameters of the Hamiltonian can be obtained by fitting to *ab initio* calculations. First we consider the Te-La-Te-Bi-Te system without magnetic order. The important symmetries of this system are (1) time-reversal symmetry T , (2) reflection symmetry σ_x with x axis as the normal axis, and (3) three-fold rotation symmetry C_3 along the z axis. In the basis of $|B_+, \frac{1}{2} \downarrow\rangle, |T_+, \frac{3}{2} \uparrow\rangle, |B_-, -\frac{1}{2} \uparrow\rangle$ and $|T_-, -\frac{3}{2} \downarrow\rangle$, the representation of the symmetry operations is given by $T = \mathcal{K} \cdot i\sigma^y \otimes \tau^z$, $\sigma_x = -i\sigma^x \otimes I$ and $C_3 = \exp(-i\frac{2}{3}\pi J_z)$, where \mathcal{K} is the complex conjugation operator, $\sigma^{x,y,z}$ and $\tau^{x,y,z}$ denote the Pauli matrices in the spin and orbital space, respectively and J_z is the angular momentum in z direction. For low energy effective model, we ignore the in-plane anisotropy and impose continuous rotational symmetry $R(\theta) = \exp(-i\theta J_z)$. By requiring these three symmetries, we obtain the following generic form of the effective Hamiltonian:

$$\mathcal{H}_0 = \begin{pmatrix} \mathcal{M}(\mathbf{k}) & Ak_+ & -i\Delta_e k_- & A'k_-^2 \\ Ak_- & -\mathcal{M}(\mathbf{k}) & A'k_-^2 & 0 \\ i\Delta_e k_+ & A'k_+^2 & \mathcal{M}(\mathbf{k}) & Ak_- \\ A'k_+^2 & 0 & Ak_+ & -\mathcal{M}(\mathbf{k}) \end{pmatrix} + \epsilon_0(\mathbf{k}) \quad (1)$$

with $k_{\pm} = k_x \pm ik_y$, $\epsilon_0(\mathbf{k}) = C_0 + D(k_x^2 + k_y^2)$, $\mathcal{M}(\mathbf{k}) = M_0 + B(k_x^2 + k_y^2)$. The block diagonal part is just the BHZ model⁵, and the off-block diagonal $\pm i\Delta_e k_{\pm}, A'k_{\pm}^2$ terms breaks the inversion

symmetry. Next we add the ferromagnetic exchange term which breaks time reversal symmetry,

$$\mathcal{H}_{ex} = \begin{pmatrix} -g_B M & & & \\ & g_T M & & \\ & & g_B M & \\ & & & -g_T M \end{pmatrix} \quad (2)$$

with g_B and g_T as Landé- g factors for two different orbitals and M the exchange field introduced by the FM ordering of Gd with half-occupied f electrons. Then the full Hamiltonian can be written as $\mathcal{H} = \mathcal{H}_0 + \mathcal{H}_{ex}$. By fitting the energy spectrum of the effective Hamiltonian with that of the *ab initio* calculations, the parameters in the effective model can be determined. For GdBiTe₃, our fitting leads to $M_0 = 27\text{meV}$, $A = 2.1\text{eV}\text{\AA}$, $B = 7.1\text{eV}\text{\AA}^2$, $C_0 = -14\text{meV}$, $D = 4.9\text{eV}\text{\AA}^2$, $A' \approx 0$, $\Delta_e = 1.1\text{eV}\text{\AA}$, $g_B M = 18\text{meV}$ and $g_T M = 59\text{meV}$, which agree well with the *ab initio* results. Such an effective model can be used for illustration of the formation of the GdBiTe₃ QAH system. As shown in Fig. 2c-e, when we have no FM ordering, the fact that $M_0, B > 0$ suggests it is the topologically trivial insulator as SQL LaBiTe₃, and the lack of inversion symmetry splits the double degeneracy except at Γ point. As we adiabatically increase the exchange field M , the $|B_+, \frac{1}{2} \downarrow\rangle$ and $|T_+, \frac{3}{2} \uparrow\rangle$ states start to move towards each other. At the transition point, those two bands form a 2D Dirac cone, and as we further increase the exchange field, those two bands become inverted and the Ak_{\pm} term hybridizes them and creates a band gap again. In this process, a topological phase transition of SQL GdBiTe₃ is shown clearly from a topologically trivial phase to the QAH phase.

Our theoretical calculations show that a SQL of GdBiTe₃ is a 2D stoichiometric magnetic

topological insulator, realizing the long-sought-after QAH state. This topological material can be grown by MBE, or by exfoliating the bulk crystal. In addition, YBiTe_3 with the same structure is found to be a normal insulator²¹, and could serve as the best substrate for MBE growth. Experimentally, the best way to see the QAH effect is to measure the four-terminal Hall conductance as a function of gate voltage. A quantized plateau in Hall conductance should be observed when the chemical potential is inside the gap. These intrinsic QAH materials could be used for applications with dissipationless electronic transport.

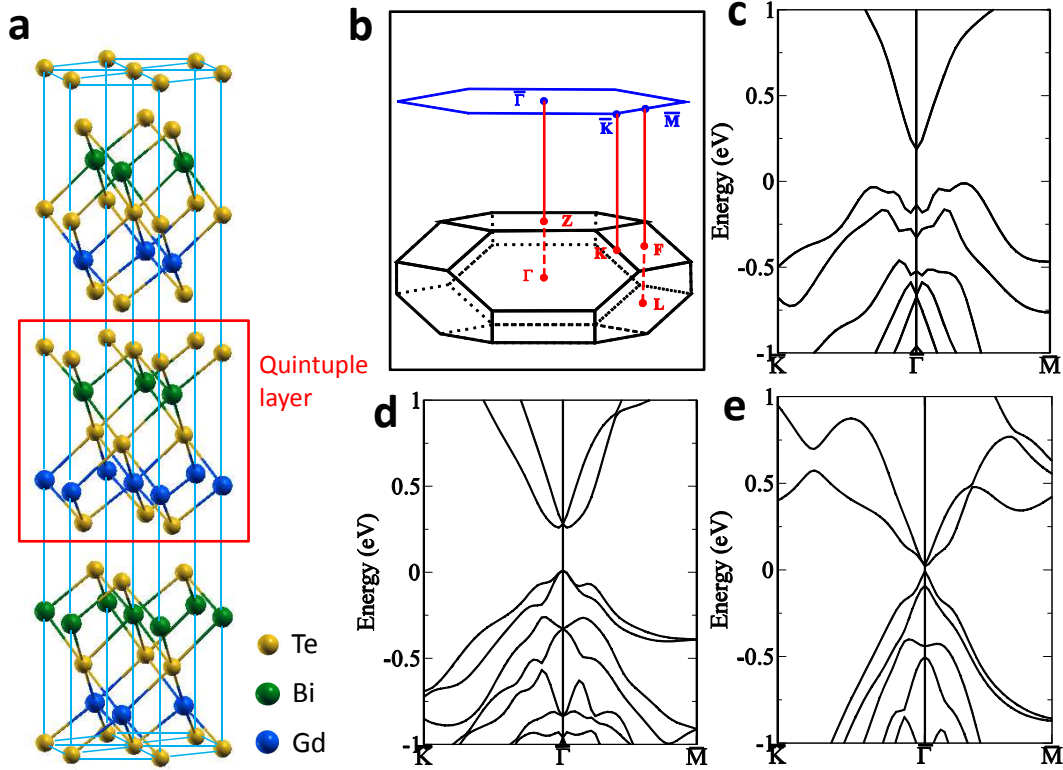


Figure 1: | **Crystal Structure, Brillouin zone and band structure.** **a**, Bulk crystal structure of GdBiTe_3 . A quintuple layer (QL) with $\text{Te1} - \text{Bi} - \text{Te2} - \text{Gd} - \text{Te1}'$ is indicated by the red box. **b**, Brillouin zone for GdBiTe_3 with space group $R\bar{3}m$, which has four inequivalent time-reversal-invariant points $\Gamma(0, 0, 0)$, $L(\pi, 0, 0)$, $F(\pi, \pi, 0)$ and $Z(\pi, \pi, \pi)$. The projected (111) 2D Brillouin zone is marked by the blue hexagon with its high-symmetry \mathbf{k} points $\bar{\Gamma}$, \bar{K} and \bar{M} . **c**, **d**, **e**, Band structure with spin-orbit coupling (SOC) for **(c)** single QL Bi_2Te_3 , **(d)** single QL LaBiTe_3 and **(e)** single QL GdBiTe_3 . The Fermi level is fixed at 0eV .

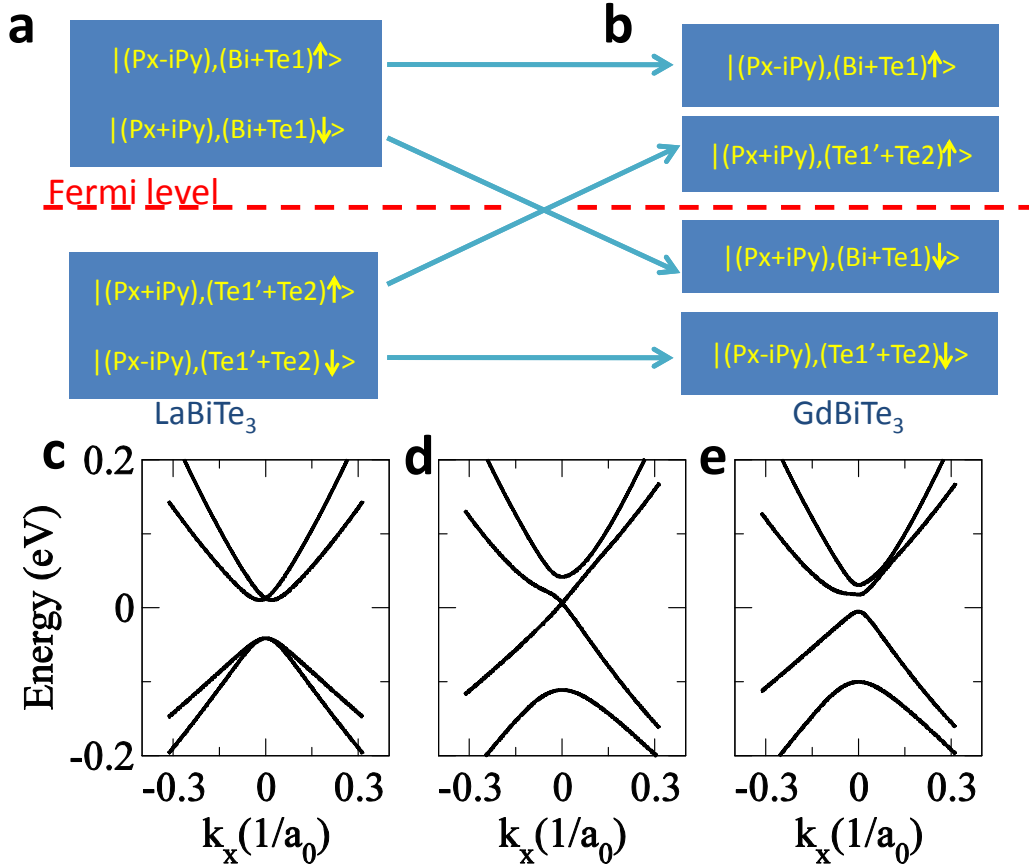


Figure 2: **Schematic representation of the topological phase transition.** **a,b**, The phase transition from **(a)** the topologically trivial insulator phase of LaBiTe₃ to **(b)** the topologically non-trivial QAH phase of GdBiTe₃. Because of the Kramers degeneracy, $|p_x - ip_y, Bi + Te1, \uparrow\rangle$ and $|p_x + ip_y, Bi + Te1, \downarrow\rangle$ states at the bottom of the conduction band, as well as states $|p_x + ip_y, Te1' + Te2, \uparrow\rangle$ and $|p_x - ip_y, Te1' + Te2, \downarrow\rangle$ at the top of the valence band are double degenerated for LaBiTe₃. The time-reversal symmetry is broken for GdBiTe₃ because of the ferromagnetism of Gd with the half filled **f** bands. The Kramers degeneracy at Γ is removed. Due to the large SOC and the ferromagnetic moment, the band inversion occurs between $|p_x + ip_y, Bi + Te1, \downarrow\rangle$ and $|p_x + ip_y, Te1' + Te2, \uparrow\rangle$. **c,d,e**, Phase transition based on the Low-energy effective model. The Kramers degeneracy at $\bar{\Gamma}$ for LaBiTe₃ is shown in the band structure **(c)** with the time-reversal symmetry, but the Kramers degeneracy for the band structure of **(e)** GdBiTe₃ is broken due to the lack of the time-reversal symmetry. The gapless Dirac-type dispersion is shown in **(d)** the band structure at the phase transition point.

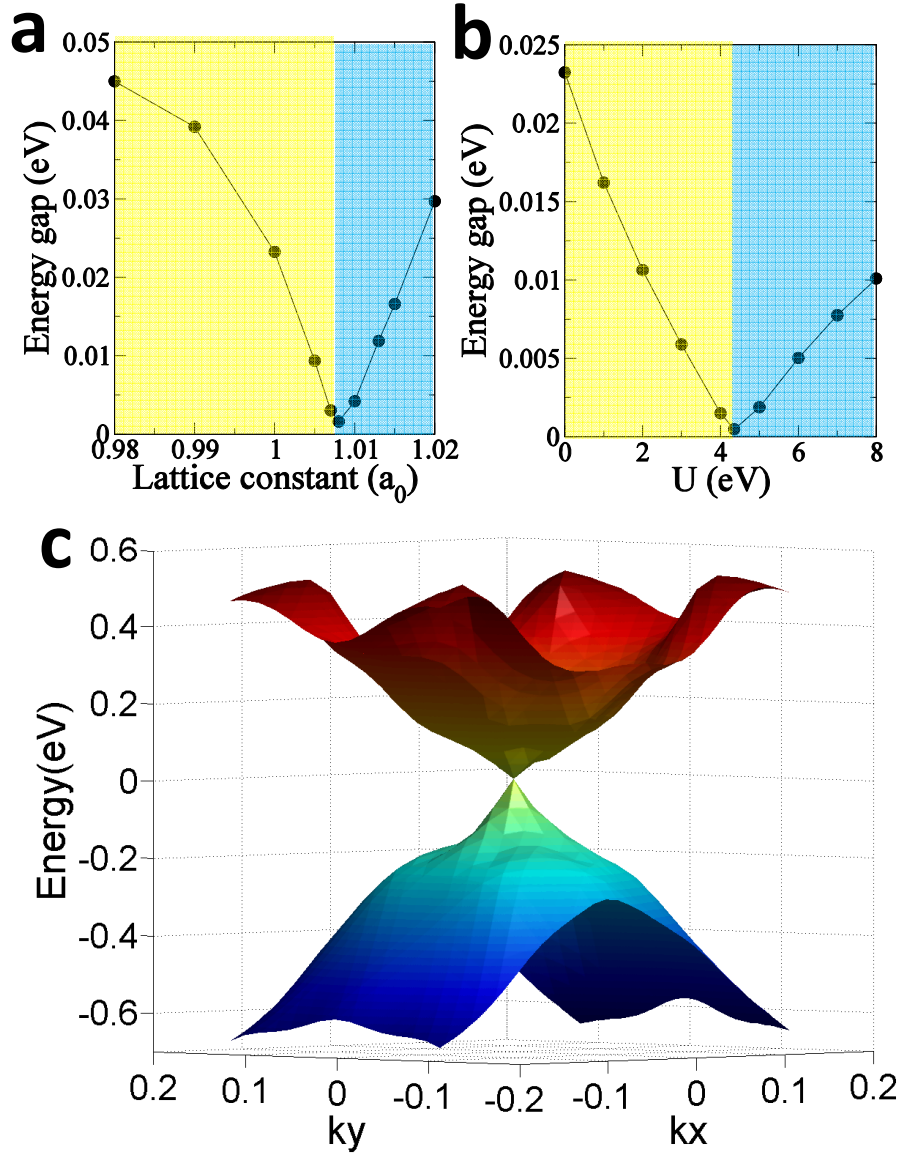


Figure 3: **Phase diagram.** **a**, The topological phase diagram depending on the lattice constant. a_0 is GdBiTe₃'s experimental bulk lattice constant. The system is in topologically non-trivial QAH phase with the small lattice constant ($a < 1.008a_0$) marked by yellow, and it becomes topologically trivial ferromagnetic insulator with the large lattice constant ($a > 1.008a_0$) marked by blue. **b**, The topological phase diagram depending on the correlation U with fixed experimental lattice constant a_0 . The GdBiTe₃ is in QAH phase with small U ($< 4.3\text{eV}$), and it changes to the topologically trivial ferromagnetic insulator phase with large U ($> 4.3\text{eV}$). **c**, The 2D Dirac-type dispersion of the lowest conduction band and the highest valence band at the transition point.

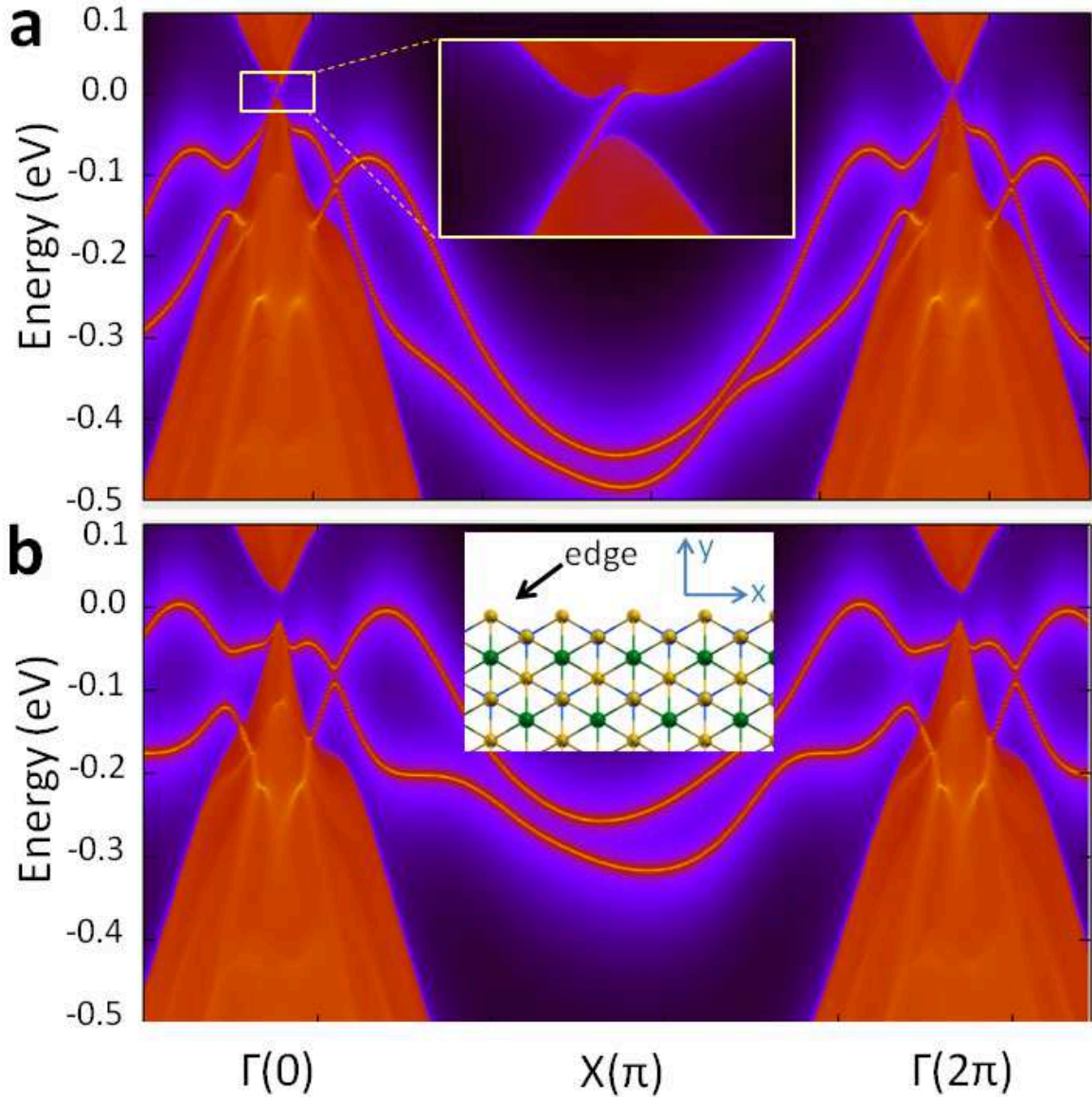


Figure 4: |**Edge states a,b**, Energy and momentum dependence of the LDOS for GdBiTe₃ with (a) QAH phase, and with (b) topologically trivial ferromagnetic insulator phase. The red regions indicate the 2D bulk bands and the dark blue regions indicate the bulk energy gap. The edge states are clearly shown in the bulk energy gap. The edge states in (a), which connect the bulk conduction bands and the bulk valence bands, are chiral, and the detailed dispersions around $\bar{\Gamma}$ are zoomed in in the inset. Comparing with the case of QAH, (b) the topologically trivial ferromagnetic insulator phase has no chiral edge states. The edge of the single QL is taken to be along x direction, which is the normal axis of the reflection symmetric plane, shown in the inset of (b).

1. Qi, X.-L. & Zhang, S.-C. The quantum spin Hall effect and topological insulators. *Physics Today* **63**, 33 (2010).
2. Hasan, M. Z. & Kane, C. L. Colloquium: Topological insulators. *Rev. Mod. Phys.* **82**, 3045–3067 (2010).
3. Moore, J. E. The birth of topological insulators. *Nature* **464**, 194–198 (2010).
4. Qi, X. L. & Zhang, S. C. Topological insulators and superconductors. *arXiv: 1008.2026v1* (2010).
5. Bernevig, B. A. , Hughes, T. L. & Zhang, S. C. Quantum spin Hall effect and topological phase transition in HgTe quantum wells. *Science* **314**, 1757 (2006).
6. König, M. *et al.* Quantum spin Hall insulator state in HgTe quantum wells. *Science* **318**, 766–770 (2007).
7. Kane, C. L. & Mele, E. J. Z_2 topological order and the quantum spin Hall effect. *Phys. Rev. Lett.* **95**, 146802 (2005).
8. Qi, X. L., Wu, Y. S. & Zhang, S. C. Topological quantization of the spin Hall effect in two-dimensional paramagnetic semiconductors. *Phys. Rev. B* **74**, 045125 (2006).
9. Liu, C.-X., Qi, X.-L., Dai, X., Fang, Z. & Zhang, S.-C. Quantum anomalous Hall effect in $\text{Hg}_{1-y}\text{Mn}_y\text{Te}$ quantum wells. *Phys. Rev. Lett.* **101**, 146802 (2008).
10. Yu, R. *et al.* Quantized anomalous Hall effect in magnetic topological insulators. *Science* **329**, 61–64 (2010).

11. Qi, X.-L., Hughes, T. L. & Zhang, S.-C. Topological field theory of time-reversal invariant insulators. *Phys. Rev. B* **78**, 195424–43 (2008).
12. Nagaosa, N., Sinova, J., Onoda, S., MacDonald, A. H. & Ong, N. P. Anomalous Hall effect. *Rev. Mod. Phys.* **82**, 1539–1592 (2010).
13. Haldane, F. D. M. Model for a quantum Hall effect without landau levels: Condensed-matter realization of the "parity anomaly". *Phys. Rev. Lett.* **61**, 2015–2018 (1988).
14. Onoda, M. & Nagaosa, N. Quantized anomalous Hall effect in two-dimensional ferromagnets: Quantum Hall effect in metals. *Phys. Rev. Lett.* **90**, 206601 (2003).
15. Liu, Q., Liu, C.-X., Xu, C., Qi, X.-L. & Zhang, S.-C. Magnetic impurities on the surface of a topological insulator. *Phys. Rev. Lett.* **102**, 156603 (2009).
16. Chen, Y. L. *et al.* Massive dirac fermion on the surface of a magnetically doped topological insulator. *Science* **329**, 659–662 (2010).
17. Dietl, T., Ohno, H., Matsukura, F., Cibert, J. & Ferrand, D. Zener model description of ferromagnetism in zinc-blende magnetic semiconductors. *Science* **287**, 1019–1022 (2000).
18. Zhang, H. *et al.* Topological insulators in Bi_2Se_3 , Bi_2Te_3 and Sb_2Te_3 with a single dirac cone on the surface. *Nature Physics* **5**, 438–442 (2009).
19. Xia, Y. *et al.* Observation of a large-gap topological-insulator class with a single dirac cone on the surface. *Nature Physics* **5**, 398–402 (2009).

20. Chen, Y. L. *et al.* Experimental realization of a three-dimensional topological insulator, Bi_2Te_3 . *Science* **325**, 178–181 (2009).
21. Yan, B. *et al.* Theoretical prediction of topological insulator in ternary rare earth chalcogenides. *Phys. Rev. B* **82**, 161108 (2010).
22. Madelung, O., Rossler, U. & M., S. GdBiTe_3 crystal structure. *Landolt-Bornstein - Group III Condensed Matter - Numerical Data and Functional Relationships in Science and Technology: 41E: Ternary Compounds, Organic Semiconductors* .
23. Perdew, J. P., Burke, K. & Ernzerhof, M. Generalized gradient approximation made simple. *Phys. Rev. Lett.* **77**, 3865 (1996).
24. Fang, Z. & Terakura, K. Structural distortion and magnetism in transition metal oxides: crucial roles of orbital degrees of freedom. *Journal of Physics: Condensed Matter* **14**, 3001–3014 (2002).
25. Anisimov, V. I., Solovyev, I. V., Korotin, M. A., Czyżyk, M. T. & Sawatzky, G. A. Density-functional theory and nio photoemission spectra. *Phys. Rev. B* **48**, 16929–16934 (1993).
26. Mauger, A. & Godart, C. The magnetic, optical, and transport properties of representatives of a class of magnetic semiconductors: The europium chalcogenides. *Physics Reports* **141**, 51 – 176 (1986).
27. Mitra, C. & Lambrecht, W. R. L. Magnetic exchange interactions in the gadolinium pnictides from first principles. *Phys. Rev. B* **78**, 134421 (2008).

28. Li, Y.-Y. *et al.* Intrinsic topological insulator Bi_2Te_3 thin films on Si and their thickness limit. *Advanced Materials* **22**, 4002–4007 (2010).
29. Marzari, N. & Vanderbilt, D. Maximally localized generalized wannier functions for composite energy bands. *Phys. Rev. B* **56**, 12847 (1997).
30. Sancho, M. P. L., Sancho, J. M. L., Sancho, J. M. L. & Rubio, J. Highly convergent schemes for the calculation of bulk and surface green functions. *Journal of Physics F: Metal Physics* **15**, 851–858 (1985).

Acknowledgements We are indebted to B.H. Yan at University of Bremen, X.L. Qi and Q.F. Zhang at Stanford University for their great help. We would like to thank Y.L. Chen and D.S. Kong for their useful discussion. This work is supported by the Army Research Office (No.W911NF-09-1-0508) and the Keck Foundation.

Competing Interests The authors declare that they have no competing financial interests.

Correspondence Correspondence and requests for materials should be addressed to Shou-Cheng Zhang (email:sczhang@stanford.edu).